ICASSP 2026 - 2026 IEEE International Conference on Acoustics, Speech and Signal Processing (ICASSP) | 979-8-3315-6701-9/26/$31.00 ©2026 IEEE | DOI: 10.1109/ICASSP55912.2026.11462366

DEEP TENSOR COMPLETION FOR FAST DIRECT POSITION DETERMINATION

Hongcheng Dong[⋆†‡] *Wenqiang Pu*[⋆†‡] *Rui Zhou*[⋆†‡] *Feng Yin*[§] *Xiao Fu*[†]

[⋆] Shenzhen Research Institute of Big Data, Shenzhen, China
[†] Shenzhen International Center for Industrial and Applied Mathematics, Shenzhen, China
[‡] School of Science and Engineering, The Chinese University of Hong Kong, Shenzhen, China
[§] School of Artificial Intelligence, The Chinese University of Hong Kong, Shenzhen, China
[†]School of Electrical Engineering and Computer Science, Oregon State University, Corvallis, USA

ABSTRACT

Direct position determination (DPD) is one powerful technique for emitter localization especially under low signal-to-noise ratio conditions, but its practical use is hindered by the prohibitive computational cost of its exhaustive grid search. To overcome this limitation, this work proposes a structured tensor completion-based approach, in which the high-dimensional DPD likelihood tensor is approximately modeled as the sum of a rank-one unimodal tensor plus a low-rank background tensor. A specialized deep neural network (DNN) is then designed to learn the factors of this decomposition directly from sparse observations, eliminating the need for a full grid search. Experiments reveal that our structure-based approach can successfully translate a low reconstruction error into an accurate state estimate, a task that generic DNN baselines fail at. Such a computationally efficient framework makes high-performance DPD practical for real-time applications.

***Index Terms*—** Direct Position Determination (DPD), CP Decomposition, Tensor Completion, Deep Neural Network

1. INTRODUCTION

Over the past decades, passive localization has evolved into a critical technology with a broad range of applications, including electronic reconnaissance [1], rescue operations [2] and autonomous driving [3]. Existing passive localization approaches can generally be divided into two main categories: one is two-step indirect methods that rely on intermediate parameter estimation, and the other is Direct Position Determination (DPD) [4] methods that estimate the emitter's position directly from the raw sensor data.

The two-step approach first extracts position-dependent parameters, such as time difference of arrival (TDOA) [5], angle of arrival (AOA) [6], or received signal strength (RSS) [7], and then estimates the emitter position by solving an optimization problem constructed from these parameters. This method is often suboptimal, especially under low signal-to-noise ratio (SNR) conditions, because it fails to enforce the crucial constraint that all parameter estimates must correspond to the same source position [8]. In contrast, DPD [9, 10, 11, 12] directly estimates the source position by jointly modeling the signals from all sensors as a function of a candidate state (position and velocity). This avoids intermediate parameter extraction and generally achieves better accuracy. However, the performance of DPD is critically dependent on an exhaustive search over a discretized grid, and achieving sufficient resolution leads to prohibitive computational costs, which remains a significant barrier to its practical application.

Recent efforts to reduce the computational cost of DPD have primarily followed two paths. The first involves end-to-end learning, where deep neural networks (DNNs) map raw received signals directly to source position [13, 14, 15, 16]. While this path enables fast position estimation, it overlooks the intrinsic physical structure of the DPD paradigm, resulting in black-box models with limited interpretability. The second path exploits structural properties of the DPD output, for instance, in two-dimensional scenarios, low-rank matrix completion has been used to accelerate computation by leveraging the approximately low-rank structure of the likelihood landscape [17]. However, this approach does not naturally extend to higher-dimensional problems, where the DPD likelihood landscape forms a high-order tensor whose complex structure cannot be adequately captured by simple low-rank models.

To close this gap, we propose a structured tensor model to represent the high-dimensional DPD likelihood landscape, in which low-dimensional factor representations are learned by DNNs. This allows for efficient inference of position and velocity from fewer samples. Our contributions are summarized as follows:

- **A Canonical Polyadic decomposition (CPD [18, 19])-Structured Tensor Model:** We introduce a model that approximates the DPD likelihood tensor as the sum of a rank-one unimodal tensor for state determination and a low-rank tensor for the background compensation. This principled approach converts the high-dimensional exhaustive search into a structured tensor completion problem, which only requires sampling a few elements of the tensor.
- **A structural DNN for Tensor Completion:** We design an efficient and structural DNN to learn the solution of the proposed tensor completion problem. The DNN is trained offline and can be efficiently implemented to infer emitter state from few samples. This yields a fast inference way to attain the solution while preserving the structure of the DPD tensor.

2. BACKGROUND AND PROPOSED FORMULATION

2.1. The Direct Position Determination (DPD) Paradigm

To determine the state of a signal source (e.g., position $\boldsymbol{x}$ and velocity $\boldsymbol{v}$) from signal samples received by M stationary sensors, one powerful approach is the DPD framework [4]. Grounded in the physical principles of signal propagation and a Maximum Likelihood (ML) criterion [4], the DPD framework directly correlates raw

Corresponding Author: Wenqiang Pu and Rui Zhou.

received data with hypothesized target states, bypassing intermediate parameter extraction and leveraging the full received signal for higher localization accuracy.

Mathematically, the DPD paradigm seeks to maximize a likelihood function in the state space:

$$\max_{\boldsymbol{p}\in\mathcal{P}} \max_{\boldsymbol{a}} f(\boldsymbol{a},\boldsymbol{p}) = \max_{\boldsymbol{p}\in\mathcal{P}} F(\boldsymbol{p}), \tag{1}$$

where $\boldsymbol{p} = [\boldsymbol{x}^T, \boldsymbol{v}^T]^T \in \mathbb{R}^4$ is the source state within the search space $\mathcal{P}$, and $\boldsymbol{a}$ represents unknown signal vector and channel parameters [11]. Function $F(\boldsymbol{p})$ represents the likelihood landscape over the position-velocity space, which is typically derived using ML [4] or a Generalized Likelihood Ratio Test (GLRT) [20].

The practical implementation of DPD is hindered by a prohibitive computational cost. First, evaluation of $F(\boldsymbol{p})$ at every grid involves computationally intensive operations, such as finding the largest eigenvalue [4, 12], or calculating the likelihood ratio via an iterative algorithm [21]. Second, the total number of grids grows exponentially with the state dimension, i.e., $\mathcal{O}(G^D)$, where G is the number of grids per dimension and D is the state dimension.

2.2. Motivation

Our key insight is that the highly structured nature of the likelihood landscape $F(\boldsymbol{p})$ can help us avoid this exhaustive search. As illustrated in the two-dimensional example in Figure 1, the landscape is characterized by a dominant peak at the true source position, surrounded by a decay pattern. This structured pattern is a strong prior but has never been exploited in the literature before; leveraging such structure requires a rigorous formulation especially for the high-dimensional case.

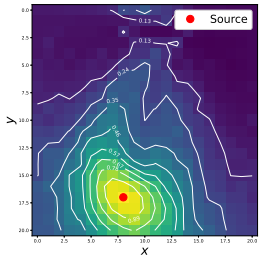

Fig. 1: A 2D contour map of the DPD likelihood landscape $F(\boldsymbol{p})$, illustrating the distinct unimodal peak at the true source position.

The DPD likelihood landscape on a discretized grid can be regarded as a high-order tensor, which exhibits a fundamental structural property dominated by a rank-one component, which can be extracted using Canonical Polyadic Decomposition (CPD). As shown in Figure 2, the factors of this dominant component are distinctly unimodal, with their peaks directly indicating the true coordinates of the source position and velocity.

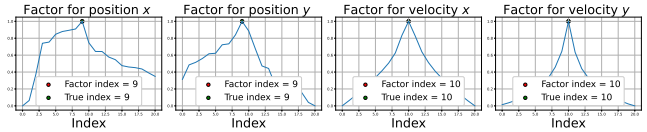

Fig. 2: The unimodal factors of the dominant rank-one component of DPD tensor. The peak location of each factor directly corresponds to a coordinate of the source's state.

Notably, the tensor's background (defined as a tensor minus its rank-one component) is evidently low-rank, a property evidenced by the sharp decay of its CPD weights after the primary component. This motivates us to model the background using a low-rank approximation. The effectiveness of this approximation can be verified on key tensor slices, though these figures are omitted due to page limitations.

2.3. Proposed Structured Tensor Completion

Based on these structural properties, we propose to reformulate the DPD grid search as a structured tensor completion problem, where the position and velocity of the source are indicated by the unimodal factors. In particular, the ground-truth likelihood tensor is denoted as $\underline{\boldsymbol{X}}^\natural \in \mathbb{R}^{I_1\times\cdots\times I_4}$. Its entries are evaluated on a discretized grid $\mathcal{G}$ of candidate states, and I_n is the number of grid points along the n-th dimension. Leveraging the structural prior, we decompose $\underline{\boldsymbol{X}}^\natural$ into three distinct CP-structured components as

$$\underline{\boldsymbol{X}}^\natural = \underline{\boldsymbol{T}} + \underline{\boldsymbol{L}} + \underline{\boldsymbol{N}}, \tag{2}$$

where $\underline{\boldsymbol{T}} = \boldsymbol{t}^{(1)} \circ \boldsymbol{t}^{(2)} \circ \boldsymbol{t}^{(3)} \circ \boldsymbol{t}^{(4)}$ is a rank-one CP tensor with a unimodality to capture the sharp peak, $\underline{\boldsymbol{L}} = \sum_{r=1}^{R_L} \boldsymbol{\ell}^{(1)}(:,r) \circ \boldsymbol{\ell}^{(2)}(:,r) \circ \boldsymbol{\ell}^{(3)}(:,r) \circ \boldsymbol{\ell}^{(4)}(:,r)$ is a low-rank CP tensor to model the structured background, and $\underline{\boldsymbol{N}}$ represents a noise tensor. Here, $\circ$ denotes the outer product of vectors, each $\boldsymbol{t}^{(n)} \in \mathbb{R}^{I_n}$ is a unimodal factor vector, and each $\boldsymbol{\ell}^{(n)} \in \mathbb{R}^{I_n \times R_L}$ is a factor matrix with R_L denoting the CP rank of $\underline{\boldsymbol{L}}$.

Instead of exhaustively evaluating all elements of this high-dimensional tensor $\underline{\boldsymbol{X}}^\natural$, we only sample a sparse subset as

$$\underline{\boldsymbol{Y}}_{\text{obs}} = \underline{\boldsymbol{O}} \circledast \underline{\boldsymbol{X}}^\natural, \tag{3}$$

where $\underline{\boldsymbol{O}}$ is a binary mask and $\circledast$ denotes the Hadamard product. The objective is thus to recover the factors of both $\underline{\boldsymbol{T}}$ and $\underline{\boldsymbol{L}}$ from the sparse observations $\underline{\boldsymbol{Y}}_{\text{obs}}$. The source state is then determined by locating the maximum in each unimodal factor vector:

$$\hat{\boldsymbol{p}}_n = \arg\max_{i\in[I_n]} \left[\boldsymbol{t}^{(n)}\right]_i, \quad \text{for } n = 1,\ldots,4. \tag{4}$$

Note that traditional model-based tensor completion methods rely on generic priors and thus struggle to capture intricate and highly nonlinear patterns in the DPD likelihood landscape $F(\boldsymbol{p})$. Instead, DNNs can effectively learn how to approximate these intricate structures directly from data. To this end, we propose a deep completion model that learns the two mapping functions:

$$\begin{aligned}(\boldsymbol{t}^{(1)},\boldsymbol{t}^{(2)},\boldsymbol{t}^{(3)},\boldsymbol{t}^{(4)}) &= g_T(g_E(\underline{\boldsymbol{Y}}_{\text{obs}};\theta_E);\theta_T),\\ (\boldsymbol{\ell}^{(1)},\boldsymbol{\ell}^{(2)},\boldsymbol{\ell}^{(3)},\boldsymbol{\ell}^{(4)}) &= g_L(g_E(\underline{\boldsymbol{Y}}_{\text{obs}};\theta_E);\theta_L),\end{aligned} \tag{5}$$

which generate the factors of the rank-one and low-rank components. Here, $g_E(\cdot;\theta_E)$ denotes the encoder function (parameterized by θ_E) that extracts a latent representation, while θ_T and θ_L represent the trainable parameters of the rank-one and low-rank decoding branches, respectively.

The complete tensor estimate is then given by:

$$\hat{\underline{\boldsymbol{X}}} = \underbrace{\boldsymbol{t}^{(1)} \circ \boldsymbol{t}^{(2)} \circ \boldsymbol{t}^{(3)} \circ \boldsymbol{t}^{(4)}}_{\underline{\boldsymbol{T}}} + \underbrace{[\![\boldsymbol{\ell}^{(1)},\boldsymbol{\ell}^{(2)},\boldsymbol{\ell}^{(3)},\boldsymbol{\ell}^{(4)}]\!]}_{\underline{\boldsymbol{L}}}. \tag{6}$$

In summary, the low-rank component $\underline{\boldsymbol{L}}$ explains away structured background variations during learning, thereby yielding a cleaner and more discriminative peak tensor $\underline{\boldsymbol{T}}$ for inference. Our deep completion model leverages this decomposition by learning to reconstruct both components simultaneously from sparse observations. The design of the DNN architecture to effectively learn these mappings is detailed in the following section.

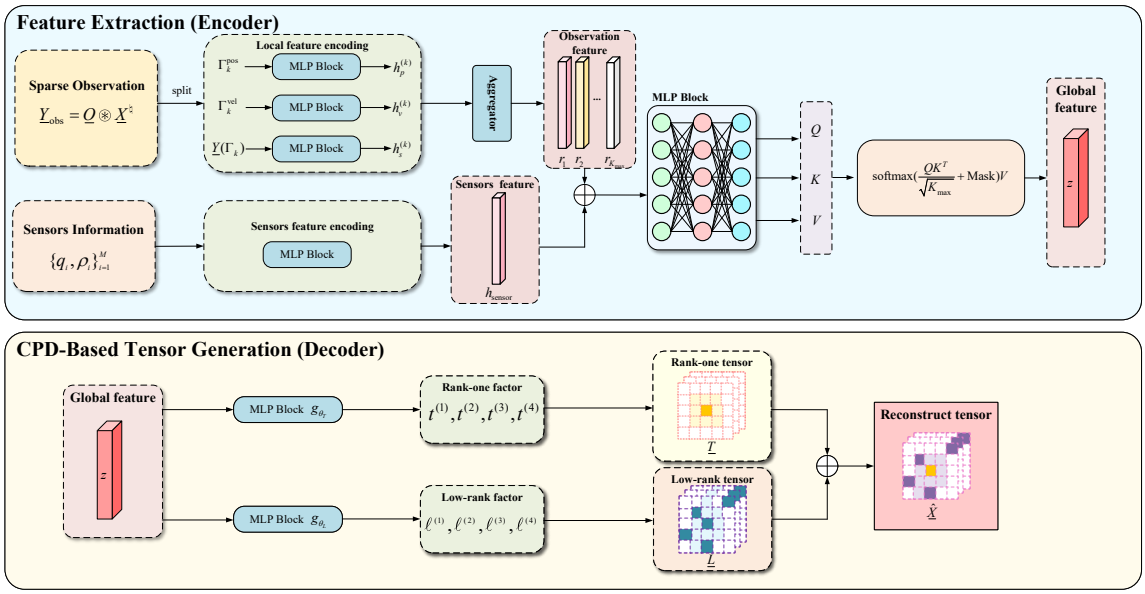

Fig. 3: Two-stage architecture of the proposed Deep Structured Tensor Completion Network: (i) an attention-based encoder for feature extraction, and (ii) a two-branch decoder for CPD-based tensor generation.

3. DNN FRAMEWORK FOR STRUCTURED TENSOR COMPLETION

To solve the structured tensor completion problem formulated above, this section introduces the **S**tructured **T**ensor **C**ompletion for DPD (STC-DPD), which learns the CP factors of both the rank-one peak tensor $\underline{\boldsymbol{T}}$ and the low-rank background tensor $\underline{\boldsymbol{L}}$ directly from sparse observations and sensor information. The inclusion of sensor information here (e.g., sensor geometry and SNR) is crucial, as the structure of the likelihood landscape $F(\boldsymbol{p})$ is highly dependent on these physical conditions.

3.1. Network Architecture

As illustrated in Figure 3, the architecture of STC-DPD is composed of two stages. The first stage is an attention-based encoder that distills features from sparse observations, sensor geometry and SNR into a global feature. The second stage is a two-branch decoder that uses the obtained feature to generate the separate CP factors for the rank-one tensor $\underline{\boldsymbol{T}}$ and the background tensor $\underline{\boldsymbol{L}}$.

Feature Extraction (Encoder): The encoder's goal is to process the inputs and produce a global feature vector $\boldsymbol{z}$. It handles two parallel information streams. First, the encoder processes the sparse DPD observation tensor $\underline{\boldsymbol{Y}}_{\text{obs}}$, which contains $\|\underline{\boldsymbol{O}}\|_0$ non-zero entries (up to a maximum of $K_{\max}$ observations). For each index $k = 1, 2, \ldots, \|\underline{\boldsymbol{O}}\|_0$, the corresponding entry consists of a grid index $\boldsymbol{\Gamma}_k$ and its value $\underline{\boldsymbol{Y}}_{\text{obs}}(\boldsymbol{\Gamma}_k)$, which the encoding block maps to a feature vector $\boldsymbol{r}_k$. Second, the encoder processes the sensor positions $\{\mathbf{q}_i\}_{i=1}^M$ and SNRs $\{\rho_i\}_{i=1}^M$ to produce a unified sensor information vector $\boldsymbol{h}_{\text{sensor}}$. These streams are fused by concatenating each observation feature $\boldsymbol{r}_k$ with the shared sensor vector $\boldsymbol{h}_{\text{sensor}}$. Finally, a self-attention mechanism aggregates this set of fused features into the global feature $\boldsymbol{z}$, dynamically scaling the contribution of each observation.

CPD-Based Tensor Generation (Decoder): The decoder maps the global feature $\boldsymbol{z}$ to the CP factors of the final decomposition via two parallel branches, which implement the functions g_T and g_L. The rank-one branch g_T maps the global feature $\boldsymbol{z}$ to the four factor vectors $\{\boldsymbol{t}^{(n)}\}_{n=1}^4$ that form the rank-one tensor $\underline{\boldsymbol{T}}$, while the low-rank branch g_L maps $\boldsymbol{z}$ to the four factor matrices $\{\boldsymbol{\ell}^{(n)}\}_{n=1}^4$ that form the low-rank background tensor $\underline{\boldsymbol{L}}$. The final estimated DPD tensor $\hat{\underline{\boldsymbol{X}}}$ is then reconstructed by summing the two components $\underline{\boldsymbol{T}}$ and $\underline{\boldsymbol{L}}$.

Architecture Motivation: The attention-based encoder handles the variable number $\|\underline{\boldsymbol{O}}\|_0$ of non-zero observations (where $0 < \|\underline{\boldsymbol{O}}\|_0 \leq K_{\max}$) across different scenarios by dynamically weighting each observation based on its consistency with the likelihood landscape. This mechanism enables the model to focus on the most informative measurements and extract a global feature vector $\boldsymbol{z}$, which provides sufficient information for the subsequent generation of $\{\boldsymbol{t}^{(n)}\}_{n=1}^4$ and $\{\boldsymbol{\ell}^{(n)}\}_{n=1}^4$.

3.2. Training Objective

STC-DPD is trained end-to-end by minimizing a composite loss function $\mathcal{L}$ that combines a reconstruction term for data fidelity with a regularization term that incorporates our proposed structural prior. The loss is defined as

$$\mathcal{L} = \underbrace{\left\| \hat{\underline{\boldsymbol{X}}} - \underline{\boldsymbol{X}}^{\natural} \right\|_F^2}_{\text{Reconstruction Loss}} + \lambda \underbrace{\sum_{n=1}^{4} \mathcal{L}_{\text{UR}}(\boldsymbol{t}^{(n)})}_{\text{Unimodality Regularization}}, \tag{7}$$

where the reconstructed tensor $\hat{\underline{\boldsymbol{X}}} = \boldsymbol{t}^{(1)} \circ \boldsymbol{t}^{(2)} \circ \boldsymbol{t}^{(3)} \circ \boldsymbol{t}^{(4)} + [\![\boldsymbol{\ell}^{(1)}, \boldsymbol{\ell}^{(2)}, \boldsymbol{\ell}^{(3)}, \boldsymbol{\ell}^{(4)}]\!]$, with the factor vectors $\{\boldsymbol{t}^{(n)}\}_{n=1}^4$ and matrices $\{\boldsymbol{\ell}^{(n)}\}_{n=1}^4$ generated by the DNN as in (5).

The Reconstruction Loss is the squared Frobenius norm between the estimated tensor $\hat{\underline{\boldsymbol{X}}}$ and the ground-truth $\underline{\boldsymbol{X}}^{\natural}$, driving the model to accurately recover the overall likelihood landscape. The Unimodality Regularization is weighted by a hyperparameter $\lambda \geq 0$. This term enforces the physical prior that the localization peak should be unimodal. It is defined for the rank-one tensor $\underline{\boldsymbol{T}}$ as

for $n = 1, 2, 3, 4$:

$$\mathcal{L}_{\text{UR}}(\boldsymbol{t}^{(n)}) = \sum_{i=2}^{p_n^\natural} [t_{i-1}^{(n)} - t_i^{(n)}]_+ + \sum_{i=p_n^\natural+1}^{I_n} [t_i^{(n)} - t_{i-1}^{(n)}]_+, \quad (8)$$

where $[\cdot]_+ = \max(0, \cdot)$ and $p_n^\natural$ is the grid index of the true peak along the n-th dimension. This penalty function ensures that each factor vector is monotonically non-decreasing up to the peak and non-increasing thereafter. In essence, while the reconstruction loss ensures the estimated tensor fits the ground-truth, the unimodality regularization guides the network to find a solution that is physically interpretable, as illustrated by the factor profiles in Figure 2.

We remark that the proposed framework offers several key advantages over both traditional DPD and end-to-end DNN methods. Firstly, it preserves the well-studied signal processing principles for computing $F(\mathbf{p})$, ensuring physical foundations are retained. Secondly, it focuses the DNN on learning only the unmodeled landscape structure, which simplifies the learning problem and enhances interpretability. Thirdly, it embeds the intrinsic structure of the DPD tensor into the network design, achieving reliable accuracy with significantly reduced computational complexity.

4. EXPERIMENTS

This section presents a comparative evaluation of STC-DPD against representative baseline methods, along with an ablation study.

4.1. Experimental Setup

Dataset We generate a synthetic dataset comprising 1000 distinct scenarios, created from 10 distinct sensor geometries and 100 emitter state/SNR combinations per geometry. For each scenario, the received signal is simulated as a BPSK-modulated signal with 100 kHz baud rate. The carrier frequency is at 1.42 GHz and duration time of each signal trial is 0.1 s with a 600 kHz sampling rate. The DPD likelihood values are computed on a four-dimensional search grid covering a position region of $[0, 20]\,\text{km}$ and a velocity region of $[-100, 100]\,\text{m/s}$. Each dimension is discretized into 21 grid points, forming a dataset of fourth-order DPD tensors with total 21^4 entries. The likelihood values within each tensor are normalized to the range $[0, 1]$. The entire dataset is partitioned into training, validation, and test sets following a 7:2:1 ratio.

Baselines and Metrics We first compare STC-DPD against distinct learning-based tensor completion baselines:

- **MLP-based Low-Rank Model (MLRM):** A basic MLP model that outputs the factors of a low-rank CP decomposition to construct the complete tensor.
- **4D ConvNet** [22]: A generic DNN using a 4D convolutional encoder-decoder framework to learn a mapping from the sparse tensor to the complete tensor.

To evaluate the performance of STC-DPD from different perspectives, we adopt two primary metrics: (i) the **absolute state error**, defined as the Euclidean distance between the estimated and ground-truth emitter states in the discretized state space, with a grid resolution of 1 km in position and 10 m/s in velocity; and (ii) the **reconstruction loss**, which is the normalized Frobenius norm between the reconstructed and ground-truth DPD tensors.

4.2. Comparison with Baselines

We compare our proposed STC-DPD against the DPD benchmark and two DNN baselines using a fixed input observation ratio of 5%, which is defined as the ratio of observed entries to total tensor size, $\rho = \|\boldsymbol{\mathcal{O}}\|_0 / \prod_{n=1}^4 I_n$. Results in Table 1 reveal a crucial insight: although MLRM and 4D ConvNet attain low reconstruction loss, this does not guarantee accurate state estimation, as both baselines exhibit substantially higher position and velocity errors than our method. This discrepancy arises because these generic architectures, which lack specific structural priors, can approximate the overall distribution of the DPD likelihood landscape but consistently fail to model the sharp, distinct peak with the grid precision necessary for reliable localization. Moreover, without explicit structural priors, these models are prone to overfitting in the training data, leading to degraded generalization and unreliable state estimates despite low reconstruction loss.

Table 1: Comparison with baselines on the test set.

Model	Pos. Err	Vel. Err	Recon. Loss	Time Ratio
Proposed	**1.44**	**0.96**	**0.0018**	5.04%
DPD	0.52	0.27	–	100.00%
MLRM	4.80	5.56	0.0021	**5.00%**
4D ConvNet	4.38	5.03	0.0173	5.24%

In contrast, our proposed STC-DPD demonstrates a balance of performance. While its accuracy is naturally lower than the DPD benchmark derived from the full tensor, it achieves state estimation errors that are significantly closer to this ideal baseline than other learning-based methods. Critically, this performance is achieved using only 5% of the samples, reducing the computation time to 5% of the time required by the exhaustive DPD grid search under the same computational settings and hardware. Although STC-DPD is marginally slower than the MLRM baseline, the overall advantage in efficiency is substantial. By explicitly modeling the rank-one and low-rank structure and enforcing the unimodality prior, our proposed STC-DPD is guided to reconstruct not just the general landscape, but more importantly, a well-defined and correctly located peak. This structure-based design is the key to bridging the gap between a low reconstruction error and a genuinely accurate state estimate.

4.3. Ablation Studies

To validate the contributions of key components within our proposed STC-DPD, we conduct two ablation studies. Specifically, we test the efficacy of the attention mechanism and the unimodality regularization, with results summarized in Table 2.

Table 2: Ablation study of the proposed framework's components.

Model Configuration	Pos. Err	Vel. Err
Proposed	**1.44**	**0.96**
w/o Attention	2.21	2.55
w/o Unimodality Reg.	4.89	5.71

From Table 2, we observe that removal of the unimodality regularization causes the most significant performance degradation, with position and velocity errors increasing by over 240% and 490% respectively. This highlights that enforcing this physical prior is critical for guiding the network to a correct and interpretable solution. Similarly, removing the attention mechanism also substantially harms performance, confirming its crucial role in effectively aggregating information from sparse inputs.

Acknowledgment

This work was supported in part by the National Natural Science Foundation of China under Grant 62571347, and Grant 62201362, and in part by the Low-Altitude Airspace Strategic Program Portfolio under Grant Z25306102, and in part by the Shenzhen Science and Technology Program under Grant JCYJ20250604191208011, and in part by SRIBD under Grant J00120260001. The work of X. Fu was supported in part by the National Science Foundation (NSF) under Project NSF ECCS-20240.

5. REFERENCES

[1] J. Matuszewski and A. Dikta, "Emitter location errors in electronic recognition system," in *Proceedings of the XI Conference on Reconnaissance and Electronic Warfare Systems*. SPIE, 2017, vol. 10418, pp. 99–106.

[2] P. Georgopoulos, B. McCarthy, and C. Edwards, "Location awareness rescue system: Support for mountain rescue teams," in *Proceedings of the 2010 Ninth IEEE International Symposium on Network Computing and Applications*. IEEE, 2010, pp. 243–246.

[3] J. Li, P. Li, P. Li, L. Tang, X. Zhang, and Q. Wu, "Self-position awareness based on cascade direct localization over multiple source data," *IEEE Transactions on Intelligent Transportation Systems*, vol. 25, no. 1, pp. 796–804, 2022.

[4] A.J. Weiss, "Direct position determination of narrowband radio frequency transmitters," *IEEE Signal Processing Letters*, vol. 11, no. 5, pp. 513–516, 2004.

[5] S. Stein, "Algorithms for ambiguity function processing," *IEEE Transactions on Acoustics, Speech, and Signal Processing*, vol. 29, no. 3, pp. 588–599, 1981.

[6] J. Xu, M. Ma, and C.L. Law, "Aoa cooperative position localization," in *Proceedings of the IEEE GLOBECOM 2008 - 2008 IEEE Global Telecommunications Conference*. IEEE, 2008, pp. 1–5.

[7] D. Jin, F. Yin, C. Fritsche, F. Gustafsson, and A.M. Zoubir, "Bayesian cooperative localization using received signal strength with unknown path loss exponent: Message passing approaches," *IEEE Transactions on Signal Processing*, vol. 68, pp. 1120–1135, 2020.

[8] H. Yu, G. Huang, J. Gao, and B. Liu, "An efficient constrained weighted least squares algorithm for moving source location using tdoa and fdoa measurements," *IEEE Transactions on Wireless Communications*, vol. 11, no. 1, pp. 44–47, 2012.

[9] T. Tirer and A.J. Weiss, "High resolution direct position determination of radio frequency sources," *IEEE Signal Processing Letters*, vol. 23, no. 2, pp. 192–196, 2015.

[10] M. You, W. Pu, R. Zhou, Y. Ye, M. Xiao, W. Wang, and Q. Shi, "Calibration signal-assisted emitter localization under sensor position uncertainty," *IEEE Transactions on Aerospace and Electronic Systems*, vol. 61, no. 3, pp. 6913–6927, 2025.

[11] L. Zhao, W. Pu, R. Zhou, M. You, and Q. Shi, "Contextual direct position determination for path loss informed localization," *IEEE Signal Processing Letters*, vol. 32, pp. 1241–1245, 2025.

[12] A. Weiss and G.W. Wornell, "One-bit direct position determination of narrowband gaussian signals," in *2021 IEEE Statistical Signal Processing Workshop (SSP)*, 2021, pp. 466–470.

[13] R. Xia, J. Wang, B. Deng, and F. Wang, "A fast direct position determination with embedded convolutional neural network," in *Proceedings of the Wireless Algorithms, Systems, and Applications*, Cham, 2022, pp. 417–428, Springer.

[14] J. Yang, C. Han, and J. Zhang, "Direct position determination based on neural network optimized by particle swarm," in *Proceedings of the 2021 4th International Conference on Artificial Intelligence and Pattern Recognition*, New York, NY, USA, 2022, AIPR '21, pp. 424–428, ACM.

[15] X. Chen, D. Wang, Z. Liu, and Y. Wu, "A fast direct position determination for multiple sources based on radial basis function neural network," in *Proceedings of the 2018 10th International Conference on Communication Software and Networks (ICCSN)*. IEEE, 2018, pp. 381–385.

[16] X. Chen, D. Wang, J. Yin, and Y. Wu, "A direct position-determination approach for multiple sources based on neural network computation," *Sensors*, vol. 18, no. 6, 2018.

[17] Z. Zhang, W. Pu, R. Zhou, M. You, W. Wang, and J. Yan, "Efficient position determination using low-rank matrix completion," in *Proceedings of the 2024 IEEE International Conference on Signal, Information and Data Processing (ICSIDP)*. IEEE, 2024, pp. 1–5.

[18] T.G. Kolda and B.W. Bader, "Tensor decompositions and applications," *SIAM Review*, vol. 51, no. 3, pp. 455–500, 2009.

[19] W. Pu, S. Ibrahim, X. Fu, and M. Hong, "Stochastic mirror descent for low-rank tensor decomposition under non-euclidean losses," *IEEE Transactions on Signal Processing*, vol. 70, pp. 1803–1818, 2022.

[20] R. Zhang, T.J. Lim, Y. Liang, and Y. Zeng, "Multi-antenna based spectrum sensing for cognitive radios: A glrt approach," *IEEE Transactions on Communications*, vol. 58, no. 1, pp. 84–88, 2010.

[21] E. Tzoreff and A.J. Weiss, "Expectation-maximization algorithm for direct position determination," *Signal processing*, vol. 133, pp. 32–39, 2017.

[22] S. Zhang, S. Guo, W. Huang, M.R. Scott, and L. Wang, "V4d: 4d convolutional neural networks for video-level representation learning," in *Proceedings of the International Conference on Learning Representations*, 2020.